Received July 10, 2019, accepted August 5, 2019, date of publication August 9, 2019, date of current version August 27, 2019.

Digital Object Identifier 10.1109/ACCESS.2019.2934190

A Novel Distributed and Self-Organized Swarm Control Framework for Underactuated Unmanned Marine Vehicles

XIAO LIANG[1], XINGRU QU[1], NING WANG[1], (Senior Member, IEEE), YE LI[1,2], AND RUBO ZHANG[3]

[1]School of Naval Architecture and Ocean Engineering, Dalian Maritime University, Dalian 116026, China
[2]Science and Technology on Underwater Vehicle Technology, Harbin 150001, China
[3]School of Mechanical and Electrical Engineering, Dalian Minzu University, Dalian 116026, China

Corresponding author: Xiao Liang (liangxiao@dlmu.edu.cn)

This work was supported in part by the National Natural Science Foundation of China under Grant 51579022, Grant 51879023, Grant 61673084, Grant 51879057, and Grant U1806228, in part by the Fundamental Research Funds for the Central Universities of China under Grant 3132019111 and Grant 3132019002, in part by the Research Fund from Science and Technology on Underwater Vehicle Technology under Grant 6142215180102, in part by the Project of Shandong Province Higher Educational Science and Technology Program, and in part by the Open Project from the Key Laboratory of Intelligent Perception and Advanced Control of State Ethnic Affairs Commission under Grant MD-IPAC-2019103.

ABSTRACT This paper presents a novel swarm control framework for path following of multiple underactuated unmanned marine vehicles (UMVs) with uncertain dynamics and unmeasured velocities. Main contributions are as follows: (1) unlike previous master-slave formation control, a swarm system function with distributed and self-organized capability is designed; (2) a center-of-swarm (COS) guidance scheme without vehicle number constraints is proposed for swarm path following, where an improved artificial potential field (APF) using ring-shaped repulsion is further employed for collision avoidance and obstacle avoidance; (3) a nonlinear velocity observer is incorporated into the proposed swarm control framework to estimate the unmeasured velocities, thereby contributing to robust controllers based on fuzzy sliding mode against uncertain dynamics and time-varying disturbances. Simulations are carried out to illustrate the universal applicability and effectiveness of the proposed swarm control framework.

INDEX TERMS Unmanned marine vehicles, swarm control, velocity observer, center-of-swarm guidance, fuzzy sliding mode.

I. INTRODUCTION

Over the past years, cooperative control of underactuated unmanned marine vehicles (UMVs) has drawn much attention on both military and civilian applications [1]. In addition to the traditional single vehicle, cooperative control of multiple UMVs provides higher fault tolerance and wider search area in less time [2]. Unfortunately, suffering from weak communication, high hydraulic pressure and strong ocean disturbances [3], [4], UMVs have great difficulties to explore information and collect data. Therefore, developing a coordinated control framework for multiple vehicles in the presence of uncertain dynamics and time-varying disturbances has grown into an emerging research. Previous researches pertaining to cooperative control can be classified into three categories [5], virtual structure framework [6], [7], behavioral strategy [8], [9] and leader-follower mechanisms [10], [11]. However, these cooperative control techniques are limited by the pre-designed formation. Nevertheless, there exists an obvious master-slave structure among vehicles [12]–[14], thereby causing great difficulties in self-organized coordinated motion and obstacle avoidance. By virtue of the line-of-sight range and angle between the leader and followers, a continuous sliding mode control [15], [16] with parameter estimation is employed [17]. In the presence of discrete data transmission, a continuous-discrete extended Kalman filtering algorithm is proposed for each follower to estimate the leader information [18]. Besides, a network system with multiple packet dropouts using pseudo measurement and nonlinear filtering algorithm is designed in [19], whereby followers can sense the leader positions. Also, the leader-follower formation with uncertain local dynamics and uncertain leader dynamics is reported in [20], where a dynamic surface control based neural network [21] is constructed such

The associate editor coordinating the review of this article and approving it for publication was Huiping Li.

that the controller is simple and universal. However, it should be highlighted that the leader plays a crucial role in centralized control structure, and once the leader is invalid, UMVs will lose their original formation performance.

Based on backstepping technique and biological network model, followers can track the virtual leader and transform the formation to avoid obstacles [22]. Recently, artificial potential field (APF) is employed for collision avoidance and obstacle avoidance [23]–[25]. Attractive force and repulsive force are proposed in [26], which can drive vehicles to the target or away from the obstacles. Considered dynamic obstacles and unreachable targets, the distance factor and jump strategy using an optimized APF algorithm are proposed for trajectory planning [27]. Moreover, Fuzzy logic [28], [29] for obstacle avoidance is proposed to design the attractive/repulsive function for multi-agent [30]. An improved potential field using damping technology around vehicles and obstacles is proposed for collision avoidance and obstacle avoidance [31]. However, previous formation approaches and APF strategy aiming at large-scale vehicles usually suffer from flaw that cooperative control system is complicated with much condition constraints and vehicles are rebounded from obstacles, thereby an imperative is to design a distributed and self-organized cooperative control framework for UMVs.

Inspired by above observations, we propose a novel swarm control framework with collision avoidance and obstacle avoidance capability for multiple MUVs without velocity measuring instruments in the presence of uncertain dynamics and time-varying disturbances. The center-of-swarm (COS) guidance scheme is first proposed based path following for single vehicle and light-of-sight guidance. Unlike previous researches, a distributed and self-organized system function is designed rather than a centralized and fixed formation structure. The improved APF with ring-shaped repulsion is employed for collision avoidance and obstacle avoidance. Furthermore, a nonlinear velocity observer is constructed to exactly estimate unknown velocities. The robust controllers based on fuzzy sliding mode can ensure that the desired signals produced by the proposed COS guidance can be accurately followed.

The paper is organized as follows. Section II presents the preliminaries and problem formulation. Velocity observer design is developed in Section III. The swarm guidance scheme and robust controllers are addressed in Section IV and Section V, respectively. The stability analysis of the closed-loop system is provided in Section VI. Simulations are carried out in Section VII and conclusion is stated in Section VIII.

II. PRELIMINARIES AND PROBLEM FORMULATION

A. UNDERACTUATED UMV DYNAMICS

Let $\boldsymbol{\eta}_i = [x_i,\ y_i, \psi_i]^T \in R^3$ is the position vector in the earth-fixed frame, where (x_i, y_i) denotes the UMV position coordinates and ψ_i denotes the yaw angle. $\boldsymbol{v}_i = [u_i, v_i, r_i]^T \in R^3$ is the velocity vector in the body-fixed frame. Consider a multi-vehicle system that consists of n UMVs and follow the references [32], the mathematical model is employed to describe the ith UMV under the following *Assumptions*, including the kinematics

$$\dot{\boldsymbol{\eta}}_i = \boldsymbol{R}(\psi_i)\boldsymbol{v}_i \tag{1}$$

and the dynamics

$$\boldsymbol{M}_i\dot{\boldsymbol{v}}_i = -\boldsymbol{C}_i(\boldsymbol{v}_i)\boldsymbol{v}_i - \boldsymbol{D}_i(\boldsymbol{v}_i)\boldsymbol{v}_i + \boldsymbol{\tau}_i + \boldsymbol{R}^T(\psi_i)\boldsymbol{\tau}_{wi} \tag{2}$$

where $\boldsymbol{\tau}_i = [\tau_{ui},\ \tau_{vi},\ \tau_{ri}]^T \in R^3$ is the control input vector, $\boldsymbol{\tau}|_{wi} = [\tau_{wui}, \tau_{wvi}, \tau_{wri}]^T \in R^3$ denotes the time-varying disturbances in the body-fixed frame; the rotation matrix $\boldsymbol{R}(\psi_i)$, the inertia matrix $\boldsymbol{M}_i = \boldsymbol{M}_i^T \in R^{3\times 3}$ the corilois centripetal matrix $\boldsymbol{C}_i(\boldsymbol{v}_i) \in R^{3\times 3}$ and the hydrodynamic damping matrix $\boldsymbol{D}_i(\boldsymbol{v}_i) \in R^{3\times 3}$ are given by

$$\boldsymbol{R}(\psi_i) = \begin{bmatrix} cos\psi_i & -sin\psi_i & 0 \\ sin\psi_i & cos\psi_i & 0 \\ 0 & 0 & 1 \end{bmatrix} \tag{3a}$$

$$\boldsymbol{M}_i = \begin{bmatrix} m_{11} & 0 & 0 \\ 0 & m_{22} & 0 \\ 0 & 0 & m_{33} \end{bmatrix} \tag{3b}$$

$$\boldsymbol{C}_i(\boldsymbol{v}_i) = \begin{bmatrix} 0 & 0 & -m_{22}v_i \\ 0 & 0 & m_{11}u_i \\ m_{22}v_i & -m_{11}u_i & 0 \end{bmatrix} \tag{3c}$$

$$\boldsymbol{D}_i(\boldsymbol{v}_i) = \begin{bmatrix} d_u + d_{uu}|u_i| & 0 & 0 \\ 0 & d_v + d_{vv}|v_i| & 0 \\ 0 & 0 & d_r + d_{rr}|r_i| \end{bmatrix} \tag{3d}$$

Assumption 1: Ignored pitch, roll and heave motion, each UMV is equipped with a propeller and a ruder.

Assumption 2: The UMV yaw angle and position coordinates are measured, but velocities are unmeasured.

Assumption 3: The communication is not subject to time delays and each vehicle can obtain information from neighbor.

To describe the multi-vehicle motion, a swarm system function with distributed and self-organized can be designed as

$$\boldsymbol{X}_s = f_s(\boldsymbol{\eta}) \quad \text{and} \quad \dot{\boldsymbol{X}}_s = \boldsymbol{J}_s(\boldsymbol{\eta})\boldsymbol{V} \tag{4}$$

where $f_s(\boldsymbol{\eta}) = [\bar{x}, \bar{y}, \sigma]^T \in R^3$; $\boldsymbol{J}_s(\boldsymbol{\eta}) \in R^{3\times 2n}$ is the Jacobian matrix satisfying (5). V is the swarm velocity vector. $\bar{x} = \sum_{i=1}^{n} x_i \Big/ n$ and $\bar{y} = \sum_{i=1}^{n} y_i \Big/ n$ denote the swarm central positions, $\sigma = \sum_{i=1}^{n} \sqrt{(x_i - \bar{x})^2(y_i - \bar{y})^2} \Big/ n$ is the standard deviation between $(x_i,\ y_i)$ and $(\bar{x}, \bar{y})$.

$$\boldsymbol{J}_s(\boldsymbol{\eta}) = \left[\left(\frac{\partial f_{s1}(\boldsymbol{\eta})}{\partial\boldsymbol{\eta}}\right)^T, \left(\frac{\partial f_{s2}(\boldsymbol{\eta})}{\partial\boldsymbol{\eta}}\right)^T, \left(\frac{\partial f_{s3}(\boldsymbol{\eta})}{\partial\boldsymbol{\eta}}\right)^T\right]^T \tag{5}$$

Furthermore, $\boldsymbol{J}_s^+$ denotes the pseudo-inverse matrix of $\boldsymbol{J}_s$, which is employed by $\boldsymbol{J}_S^+ = \boldsymbol{J}_S^T(\boldsymbol{J}_S\boldsymbol{J}_S^T)^{-1}$ and satisfies $\boldsymbol{J}_s\boldsymbol{J}_s^+ = \boldsymbol{I}_3$.

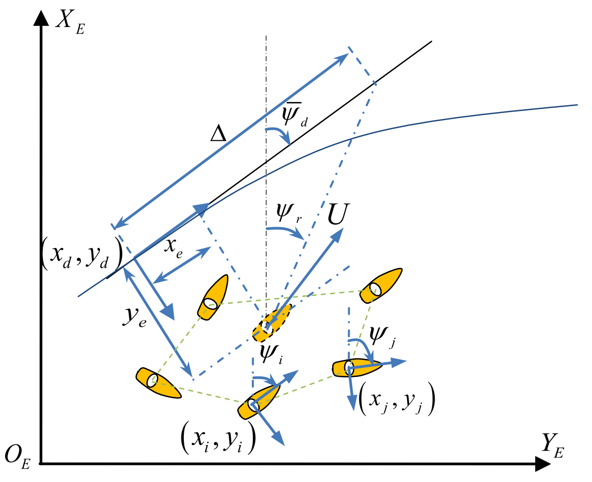

FIGURE 1. Swarm geometric structure of UMVs.

B. SWARM ERROR DYNAMICS

On the horizontal plane, the geometric structure for swarm control including multiple UMVs and a geometric path parameterized by a time-independent variable θ is shown in Fig. 1. Similar to the swarm system function (4), the desired swarm function can be described as

$$\boldsymbol{X}_d = [\bar{x}_d, \bar{y}_d, \sigma_d]^T \tag{6}$$

and the corresponding swarm errors can be expressed by

$$\boldsymbol{X}_e = \boldsymbol{X}_s - \boldsymbol{X}_d = [\bar{x} - \bar{x}_d, \bar{y} - \bar{y}_d, \sigma - \sigma_d]^T \tag{7}$$

For given θ, the path-tangent reference frame is denoted by $(x_d(\theta),\ y_d(\theta))$ which is rotated with an angle $\overline{\psi}_d$ with respect to the earth-fixed frame given by

$$\overline{\psi}_d = \text{atan2}(\dot{y}_d(\theta),\ \dot{x}_d(\theta)) \tag{8}$$

where $\dot{x}_d(\theta) = h_d/\partial\theta$ and $\dot{y}_d(\theta) = \partial y_d/\partial\theta$. For the multi-UMV system defined as (1) and (2), the along-following error x_e and cross-following error y_e between $(\bar{x}, \bar{y})$ and $(x_d(\theta),\ y_d(\theta))$ expressed in the path-tangent reference frame are described as

$$\begin{bmatrix} x_e \\ y_e \end{bmatrix} = \begin{bmatrix} cos\overline{\psi}_d & -sin\overline{\psi}_d \\ sin\overline{\psi}_d & cos\overline{\psi}_d \end{bmatrix}^T \begin{bmatrix} \bar{x} - x_d(\theta) \\ \bar{y} - y_d(\theta) \end{bmatrix} \tag{9}$$

The control objective is to design distributed controllers for each UMV with the dynamics (2), such that the swarm can follow a given geometric curved path $(x_d(\theta),\ y_d(\theta))$ and swarm errors satisfy

$$\lim_{t\to\infty} X_e \le \varepsilon_1 \tag{10}$$

and

$$\begin{cases} \lim_{t\to\infty} x_e \le \varepsilon_2 \\ \lim_{t\to\infty} y_e \le \varepsilon_3 \end{cases} \tag{11}$$

for some small constants ε_1, ε_2 and ε_3.

III. VELOCITY OBSERVER DESIGN

In this section, a nonlinear observer is developed to exactly estimate the actual UMV velocities which cannot be measured under the *Assumption 2*.

Design the velocity observer for each vehicle as follows:

$$\begin{cases} \dot{\hat{\boldsymbol{\nu}}}_i = \boldsymbol{H}_i + \boldsymbol{L}_2(\boldsymbol{\eta}_i - \hat{\boldsymbol{\eta}}_i) \\ \hat{\boldsymbol{\eta}}_i = \int_0^t (\boldsymbol{L}_1(\boldsymbol{\eta}_i - \hat{\boldsymbol{\eta}}_i) - \boldsymbol{R}(\psi_i)(\boldsymbol{\nu}_i - \hat{\boldsymbol{\nu}}_i))d\boldsymbol{\tau} + \boldsymbol{\eta}_i \\ \boldsymbol{H}_i = -\boldsymbol{M}_i^{-1}(\boldsymbol{C}_i(\hat{\boldsymbol{\nu}}_i)\hat{\boldsymbol{\nu}}_i + \boldsymbol{D}_i\hat{\boldsymbol{\nu}}_i - \boldsymbol{\tau}_i - \boldsymbol{R}^T(\psi_i)\boldsymbol{\tau}_{wi}) \end{cases} \tag{12}$$

where $\boldsymbol{L}_1 = diag\{l_{11}, l_{12}, l_{13}\}$ and $\boldsymbol{L}_2 = diag\{l_{21}, l_{22}, l_{23}\}$ are positive gain matrixes; $\hat{\boldsymbol{\eta}}_i$ and $\hat{\boldsymbol{\nu}}_i$ are the position estimation and velocity estimation; the estimation errors are further defined as

$$\tilde{\boldsymbol{\eta}}_i = \boldsymbol{\eta}_i - \hat{\boldsymbol{\eta}}_i, \quad \tilde{\boldsymbol{\nu}}_i = \boldsymbol{\nu}_i - \hat{\boldsymbol{\nu}}_i \tag{13}$$

Theorem 1: Consider UMV in (1) and (2) without velocity measuring instruments, the observer (12) can be used for unknown velocity estimation. Suppose that the control inputs are bounded and the *Assumption 2* is satisfied. Then, the estimation errors can converge to zero with global asymptotically stable.

Proof: Define observation error dynamics as follows:

$$\begin{cases} \dot{\tilde{\boldsymbol{\eta}}}_i = \boldsymbol{R}(\psi_i)\hat{\boldsymbol{\nu}}_i - \boldsymbol{L}_1\tilde{\boldsymbol{\eta}}_i \\ \dot{\tilde{\boldsymbol{\nu}}}_i = -\boldsymbol{M}_i^{-1}\boldsymbol{C}_i(\hat{\boldsymbol{\nu}}_i)\tilde{\boldsymbol{\nu}}_i - \boldsymbol{M}_i^{-1}\boldsymbol{D}_i\tilde{\boldsymbol{\nu}}_i - \boldsymbol{L}_2\tilde{\boldsymbol{\eta}}_i \end{cases} \tag{14}$$

Consider the following Lyapunov Function Candidate (LFC) as

$$V_{io} = \frac{1}{2}(\tilde{\boldsymbol{\eta}}_i^T \boldsymbol{P}_1 \tilde{\boldsymbol{\eta}}_i + \tilde{\boldsymbol{\nu}}_i^T \boldsymbol{P}_2 \tilde{\boldsymbol{\nu}}_i), \quad \forall \tilde{\boldsymbol{\eta}}_i \ne 0,\ \tilde{\boldsymbol{\nu}}_i \ne 0 \tag{15}$$

where $\boldsymbol{P}_1 = diag\{P_{11}, P_{12}, P_{13}\}$ and $\boldsymbol{P}_2 = diag\{P_{21}, P_{22}, P_{23}\}$ are positive diagonal matrixes.

Differentiating V_{io} with respect to time along (13) and (14), we have

$$\begin{aligned} \dot{V}_{io} &= (\boldsymbol{R}\tilde{\boldsymbol{\nu}}_i - \boldsymbol{L}_1\tilde{\boldsymbol{\eta}}_i)^T \boldsymbol{P}_1 \tilde{\boldsymbol{\eta}}_i + \frac{1}{2}(-L_2\tilde{\boldsymbol{\eta}}_i + \boldsymbol{\Gamma}_i\tilde{\boldsymbol{\nu}}_i)^T \boldsymbol{P}_2 \tilde{\boldsymbol{\nu}}_i \\ &\quad + \frac{1}{2}\tilde{\boldsymbol{\nu}}_i^T \boldsymbol{P}_2(-L_2\tilde{\boldsymbol{\eta}}_i + \boldsymbol{\Gamma}_i\tilde{\boldsymbol{\nu}}_i) \\ &= -\tilde{\boldsymbol{\eta}}_i^T \boldsymbol{L}_1^T \boldsymbol{P}_1 \tilde{\boldsymbol{\eta}}_i + \frac{1}{2}\tilde{\boldsymbol{\nu}}_i^T(\boldsymbol{\Gamma}_i^T \boldsymbol{P}_2 + \boldsymbol{P}_2\boldsymbol{\Gamma}_i)\tilde{\boldsymbol{\nu}}_i \\ &\quad + \tilde{\boldsymbol{\nu}}_i^T(\boldsymbol{R}^T \boldsymbol{P}_1 + \boldsymbol{P}_2(-L_2))\tilde{\boldsymbol{\eta}}_i \end{aligned} \tag{16}$$

where $\boldsymbol{\Gamma}_i = -\boldsymbol{M}_i^{-1}\boldsymbol{C}_i(\hat{\boldsymbol{\nu}}_i) - \boldsymbol{M}_i^{-1}\boldsymbol{D}_i$.

By defining

$$\begin{cases} \boldsymbol{R}^T \boldsymbol{P}_1 = \boldsymbol{P}_2 \boldsymbol{L}_2 \\ \boldsymbol{L}_1^T \boldsymbol{P}_1 = \boldsymbol{Q}_1 \\ \boldsymbol{\Gamma}_i^T \boldsymbol{P}_2 + \boldsymbol{P}_2 \boldsymbol{\Gamma}_i = 2\boldsymbol{Q}_2 \end{cases} \tag{17}$$

yields

$$\dot{\boldsymbol{V}}_{io} = -\tilde{\boldsymbol{\eta}}_i^T \boldsymbol{Q}_1 \tilde{\boldsymbol{\eta}}_i - \tilde{\boldsymbol{\nu}}_i^T \boldsymbol{Q}_2 \tilde{\boldsymbol{\nu}}_i < 0, \quad \forall \tilde{\boldsymbol{\eta}}_i \ne 0,\ \tilde{\boldsymbol{\nu}}_i \ne 0 \tag{18}$$

Furthermore, using $\sigma_1 = \lambda_{rn}(\boldsymbol{Q}_1)$, $\sigma_2 = \lambda_{rn}(\boldsymbol{Q}_2)$ and (15), we have

$$\dot{V}_{io} \le -\sigma_1\|\tilde{\boldsymbol{\eta}}_i\|^2 - \sigma_2\|\tilde{\boldsymbol{\nu}}_i\|^2 \tag{19}$$

where $\lambda_{\min}$ denotes the minimum eigenvalue.

Thus, we can get the conclusion that the estimation errors converge to zero with global asymptotically stable.

IV. CENTER-OF-SWARM GUIDANCE

In this section, we propose a center-of-swarm (COS) guidance scheme including both collision avoidance and obstacle avoidance. Based on the path following for single vehicle, a guidance scheme capable of driving the UMV formation toward and along a desired path is designed. The desired behavior is ranked as follows, with obstacle avoidance being the most important: (i) Make good progress towards the desired path; (ii) Avoid collisions and obstacles; (iii) Keep safe distance from neighbor vehicles and obstacles.

Step 1: The time derivative of x_e and y_e can be derived as

$$\begin{aligned}\dot{x}_e &= \dot{\bar{x}}\cos\bar{\psi}_d + \dot{\bar{y}}\sin\bar{\psi}_d - \dot{x}_d(\theta)\cos\bar{\psi}_d - \dot{y}_d(\theta)\sin\bar{\psi}_d \\ &\quad + \dot{\bar{\psi}}_d \underbrace{(-(\bar{x}-x_d(\theta))\sin\bar{\psi}_d + (\bar{y}-y_d(\theta))\cos\bar{\psi}_d)}_{y_e}\end{aligned} \tag{20}$$

and

$$\begin{aligned}\dot{y}_e &= -\dot{\bar{x}}\sin\bar{\psi}_d + \dot{\bar{y}}\cos\bar{\psi}_d + \dot{x}_d(\theta)\sin\bar{\psi}_d - \dot{y}_d(\theta)\cos\bar{\psi}_d \\ &\quad - \dot{\psi}_d \underbrace{((\bar{x}-x_d(\theta))\cos\bar{\psi}_d + (\bar{y}-y_d(\theta))\sin\bar{\psi}_d)}_{x_e}\end{aligned} \tag{21}$$

Substituting (2) into (20) and (11) yields

$$\begin{aligned}\dot{x}_e &= -\dot{\theta}\sqrt{x_d'^2(\theta)+y_d'^2(\theta)}\cos(\bar{\psi}_d+\phi) + u\cos(\bar{\psi}-\bar{\psi}_d) \\ &\quad - v\sin(\bar{\psi}-\bar{\psi}_d) + \dot{\bar{\psi}}_d y_e \\ &= U\cos(\bar{\psi}-\bar{\psi}_d) + \dot{\bar{\psi}}_d y_e - u_p\end{aligned} \tag{22}$$

and

$$\begin{aligned}\dot{y}_e &= \dot{\theta}\sqrt{x_d'^2(\theta)+y_d'^2(\theta)}\sin(\bar{\psi}_d+\phi) + u\sin(\bar{\psi}-\bar{\psi}_d) \\ &\quad + v\cos(\bar{\psi}-\bar{\psi}_d) - \dot{\bar{\psi}}_d x_e \\ &= U\sin(\bar{\psi}-\bar{\psi}_d) - \dot{\bar{\psi}}_d x_e\end{aligned} \tag{23}$$

where $\phi = \arctan 2(-y_d(\theta), \dot{x}_d(\theta)) = -\bar{\psi}_d$; $U = \sqrt{u^2+v^2}$ represents the COS velocity and satisfies $0 \le U \le U_{\max}$; u_p is the ideal COS velocity expressed as follows:

$$u_p = U\cos(\bar{\psi}-\bar{\psi}_d) + \delta x_e \tag{24}$$

where $\delta > 0$ is a design parameter. From (22) and (23), the angle ψ_r towards the desired path can be designed as follows:

$$\psi_r = \bar{\psi}_d(\theta) + \arctan(-y_e/l_0) \tag{25}$$

where $l_0 > 0$ denotes the look-ahead distance. Since θ is the actual path parameter variable to update, we need to acquire the relationship between θ and u_p. By using (22), we define

$$\dot{\theta} = \frac{u_p}{\sqrt{\dot{x}_d^2(\theta)+\dot{y}_d^2(\theta)}} \tag{26}$$

Consider the following LFC as

$$V_1 = \frac{1}{2}x_e^2 + \frac{1}{2}y_e^2 \tag{27}$$

Differentiating V_1 along the closed-loop error dynamics (22) and (23) yields

$$\begin{aligned}\dot{V}_1 &= x_e\dot{x}_e + y_e\dot{y}_e \\ &= x_e(-\delta x_e + \dot{\bar{\psi}}_d y_e) + y_e(U\sin(\bar{\psi}-\bar{\psi}_d) - \dot{\bar{\psi}}_d x_e) \\ &= -\delta x_e^2 + y_e U\sin(\mathrm{atan}(-y_e/l_0)) \\ &= -\delta x_e^2 - Uy_e^2/\sqrt{l_0^2+y_e^2} \\ &\le -\delta x_e^2 - \varepsilon y_e^2 \\ &\le -kV_1\end{aligned} \tag{28}$$

where $\varepsilon = U\Big/\sqrt{l_0^2+y_e^2}$ and satisfies $0 \le \varepsilon \le U_{\max}\Big/\sqrt{l_0^2+y_e^2}$; $k = 2\min\{\delta, \varepsilon\}$. *Step 2* Consider the following FLC as

$$V_2 = \frac{1}{2}\boldsymbol{X}_e^T\boldsymbol{K}_1\boldsymbol{X}_e \tag{29}$$

where $\boldsymbol{K}_1 = diag\{k_{11}, k_{22}, k_{33}\}$ is positive gain matrix. Taking the time derivate of(29) and using (7) yield

$$\dot{\boldsymbol{V}}_2 = \boldsymbol{X}_e^T\boldsymbol{K}_1(\boldsymbol{J}_s(\boldsymbol{\eta})\boldsymbol{V} - \dot{\boldsymbol{X}}_d) \tag{30}$$

To make good progress towards the desired path, the desired velocities $\boldsymbol{V}_d$ of swarm system can be designed

$$\boldsymbol{V}_d = [\boldsymbol{V}_{1d}^T, \boldsymbol{V}_{2d}^T, \ldots, \boldsymbol{V}_{nd}^T]^T = -\boldsymbol{J}_s^+(\boldsymbol{K}_1\boldsymbol{X}_e - \dot{\boldsymbol{X}}_d) \tag{31}$$

where $\boldsymbol{V}_{id} = \dot{\boldsymbol{\eta}}_{id} = [\dot{x}_{id}, \dot{y}_{id}]^T$ are the desired velocities for the *ith* UMV.

Remark 1: Different from the existing APF including both attractive force and repulsive force [33], where the control algorithm can only be employed with respect to the kinematics, and none of cooperative controllers based dynamics can result. Therefore, the proposed swarm control framework considers the dynamic controllers in section 5. *Step 3* Based on the desired velocity (31), the collision avoidance algorithm presented in [34] can be employed to modify $\boldsymbol{V}_d$ An artificial function is proposed to avoid collisions among vehicles. The APF P_{ari} is a function with the following properties:

(1) P_{ari} is differentiable and non-negative;
(2) P_{ari} reaches its maximum if $\|x_{ij}\| \to 0$;
(3) P_{ari} is decreasing nonlinearly as $0 < \|x_{ij}\| \le d_0$;
(4) P_{ari} reaches its minimum or zero if $\|x_{ij}\| \to \infty$.

where $\|x_{ij}\|$ is the distance between the *ith* and thejth vehicle, $d_0 > 0$ is the safe avoidance distance. Thus, the total repulsion fields for avoiding collision is derived as $P_{ar} = \sum_{i=1}^{n} P_{ari}$.

In addition to avoiding collision, avoiding obstacles is an integral part of this swarm control framework. Based on the traditional APF in [34], a modified repulsion field has the linear ring-shaped behavior as shown in Fig. 2. Each UMV can bypass obstacles smoothly with safe distance. By defining the distance between UMV and obstacle, the repulsive force of

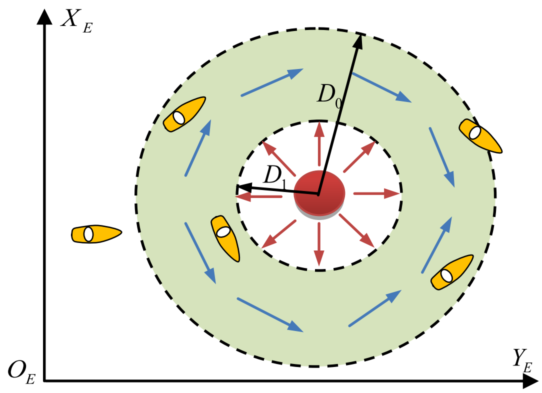

FIGURE 2. Schematic of the modified repulsion field.

obstacle collision is given by

$$\nabla P_{aoj} = \begin{cases} (\frac{1}{\|x_{oj}\|} - \frac{1}{D_0} 1 \frac{\alpha}{\|x_{oj}\|^2} \frac{\partial x_{oj}}{\partial \boldsymbol{\eta}_j'} & \text{if } \|x_{oj}\| < D_1 \\ 0, & \text{else if } \|x_{oj}\| > D_0 \\ \beta \frac{D_0 - \|x_{oj}\|}{D_0} & \text{otherwise} \end{cases} \tag{32}$$

where $\boldsymbol{\eta}_j' = [x_{oj},\ y_{oj}]^T$ is the jth obstacle, and $\beta > 0$ is the repulsion gain. $D_0 > 0$ is the maximum radius and D_1 represents the distance of the annulus repulsion field and satisfies $0 < D_1 < D_0$. Thus, the total repulsion fields for several obstacles can be derived as $P_{ao} = \sum_{j=1}^{m} P_{aoj}$.

Consider the following FLC based V_2 as

$$V_3 = \frac{1}{2}\boldsymbol{X}_e^T \boldsymbol{K}_1 \boldsymbol{X}_e + k_3 \boldsymbol{P} \tag{33}$$

where $P = k_1 \sum_{i=1}^{m} P_{aoi} + k_2 \sum_{i=1}^{n} P_{ari}$; k_1 and k_2 are positive scaling factors; k_3 is a positive constant. Taking the time derivative of V_3 yields

$$\dot{V}_3 = \boldsymbol{X}_e^T \boldsymbol{K}_1 (\boldsymbol{J}_s \boldsymbol{V} - \dot{\boldsymbol{X}}_d) + k_3 (\partial P/\partial \boldsymbol{\eta})^T \boldsymbol{V} \tag{34}$$

The desired velocity is designed as follows:

$$\begin{aligned} \boldsymbol{V}_d &= [\boldsymbol{V}_{1d}^T, \boldsymbol{V}_{2d}^T, \ldots, \boldsymbol{V}_{nd}^T]^T \\ &= -(\boldsymbol{X}_e^T \boldsymbol{K}_1 \boldsymbol{J}_s + k_3 (\partial P/\partial \boldsymbol{\eta})^T)^T + \boldsymbol{J}_s^+ \dot{\boldsymbol{X}}_d \\ &= -(k_3 \partial P/\partial \boldsymbol{\eta} + \boldsymbol{J}_s^T \boldsymbol{K}_1 \boldsymbol{X}_e) + \boldsymbol{J}_s^+ \dot{\boldsymbol{X}}_d \end{aligned} \tag{35}$$

Substituting (33) into (31) results in

$$\begin{aligned} &\dot{V}_3 \\ &= -\left(\boldsymbol{X}_e^T \boldsymbol{K}_1 \boldsymbol{J}_s + k_3 (\partial P/\partial \boldsymbol{\eta})^T\right)\left(\boldsymbol{X}_e^T \boldsymbol{K}_1 \boldsymbol{J}_s + k_3 (\partial P/\partial \boldsymbol{\eta})^T\right)^T \\ &\quad + \left(\boldsymbol{X}_e^T \boldsymbol{K}_1 \boldsymbol{J}_s + k_3 (\partial P/\partial \boldsymbol{\eta})^T\right) \boldsymbol{J}_S^+ \dot{\boldsymbol{X}}_d - \boldsymbol{X}_e^T \boldsymbol{K}_1 \dot{\boldsymbol{X}}_d \\ &= -(k_3 \partial P/\partial \boldsymbol{\eta} + \boldsymbol{J}_S^T \boldsymbol{K}_1 \boldsymbol{X}_e)^T (k_3 \partial P/\partial \boldsymbol{\eta} + \boldsymbol{J}_s^T \boldsymbol{K}_1 \boldsymbol{X}_e) \\ &\quad + k_3 (\partial P/\partial \boldsymbol{\eta})^T \boldsymbol{J}_s^+ \dot{\boldsymbol{X}}_d \\ &\leq -(k_3 \partial P/\partial \boldsymbol{\eta} + \boldsymbol{J}_S^T \boldsymbol{K}_1 \boldsymbol{X}_e)^T (k_3 \partial P/\partial \boldsymbol{\eta} + \boldsymbol{J}_s^T \boldsymbol{K}_1 \boldsymbol{X}_e) + \Delta \end{aligned} \tag{36}$$

where $k_3 > 0$, $\Delta = k_3 \left|(\partial P/\partial \boldsymbol{\eta})^T \boldsymbol{J}_s^+ \dot{\boldsymbol{X}}_d\right|$. Thereby, the center-of-swarm guidance scheme including both collision avoidance and obstacle avoidance is provided by *step 1, step 2* and *step3*. Moreover, each vehicle gives priority to keep distance with neighUors and obstacles.

V. CONTROLLER DESIGN

In this section, we design heading and surge controllers for the *ith* UMV to ensure the desired behavior. The desired surge velocity and heading angle for the *ith* vehicle are given by

$$u_{id} = \sqrt{\dot{x}_{id}^2 + \dot{y}_{id}^2}, \quad \text{and } \psi_{id} = \text{atan2}\,(\dot{y}_{id},\ \dot{x}_{id}) \tag{37}$$

A. FUZZY APPROXIMATOR

A fuzzy logic system (FLS) is employed as the universal approximator to estimate the unknown, and the detail expression of FLS is defined as

$$\begin{aligned} R^J &: if\ x_1\ is\ A_1^j\ and\ x_2\ is\ A_2^j\ \cdots\ and\ x_n\ is\ A_n^j \\ &\quad then\ y\ is\ B^j \end{aligned}$$

where R^j represents the fuzzy rules, and $j = 1, 2, k.y$ and $\boldsymbol{x} = [x_1,\ x_2, \cdots, x_n]^T$ is the output and input, respectively. 4^J and B^j are fuzzy singletons [35, 36]. Given k fuzzy rules, the total output of the fuzzy approximator is

$$y(\boldsymbol{x}) = \sum_{j=1}^{k} \xi_j(\boldsymbol{x})\theta_j = \theta^T \boldsymbol{\xi} \tag{38}$$

where $\boldsymbol{\theta} = [\theta_1, \theta_2, \cdots, \theta_k]^T$ is adjustaule parameter vector; $\boldsymbol{\xi}_j(\boldsymbol{x})$ is the membership function.

$$\boldsymbol{\xi}_j(x) = \frac{\Pi_{i=1}^n \mu_{Ai}^j(x_i)}{\sum_{j=1}^k (\Pi_{i=1}^n \mu_{Ai}^j(x_i))} \tag{39}$$

where $\mu_{Ai}^j(x_i)$ is the membership function.

Remark 2: It is worthy to indicate that, if the FLS is replaced using neural network, similar results can be conducted without any difficulty.

B. SURGE CONTROL

Consider the dynamics (2), the surge controller τ_{iu} can be chosen as

$$\begin{aligned} \tau_{iu} = -\hat{m}_{22}\hat{v}_i\hat{r}_i + \left(\hat{d}_u + \hat{d}_{uu}\left|\hat{u}_i\right|\right)\hat{u}_i - K_{iu}\,\text{sgn}\,(S_{iu}) \\ - \hat{m}_{11}\,(\lambda_{i2}u_{ie} - \dot{u}_{id}) \end{aligned} \tag{40}$$

where $\lambda_{i2} > 0$; u_{id} is the desired surge velocity computed by (37), and S_{iu} is the integral sliding surface governed by

$$S_{iu} = \lambda_{i2} \int_0^t u_{ie}(\tau_{iu}) d\tau_{iu} + u_{ie} \tag{41}$$

with $u_{ie} = \hat{u}_i - u_{id}$ is the surge error, K_{iu} is the uncertain gain function defined as

$$\begin{aligned} K_{iu} = (m_{22} - \hat{m}_{22})\hat{v}_i\hat{r}_i + \left(\left(d_u - \hat{d}_u\right) + \left(d_{uu} - \hat{d}_{uu}\right)\left|\hat{u}_i\right|\right)\hat{u}_i \\ + (m_{11} - \hat{m}_{11})(\lambda_{i2}u_{ie} - \dot{u}_{id}) + \tau_{iwu} \end{aligned} \tag{42}$$

A FLS is used to approximate the uncertain dynamics and time-varying disturbances in K_{iu}

$$\hat{K}_{iu} = \hat{\boldsymbol{\theta}}_{iu}^{T}\boldsymbol{\xi}_{iu}(\boldsymbol{x}) \tag{43}$$

where $\boldsymbol{x} = \left[\hat{u}, \hat{v}, \hat{r}\right]^T$ is the velocity vector, and $\hat{\boldsymbol{\theta}}_{iu}$ is adaptive law designed as

$$\dot{\hat{\boldsymbol{\theta}}}_{iu} = \eta_{iu}|S_{iu}|\boldsymbol{\xi}_{iu}(\boldsymbol{x}) \tag{44}$$

where $\boldsymbol{\eta}_{iu} > 0$; the corresponding membership function is selected as

$$\xi_1^j(\boldsymbol{x}) = \exp\left[-\left(\left(\boldsymbol{x} + \frac{\rho_1}{6} - (j-1)\frac{\rho_1}{12}\right)/\sigma_1\right)^2\right], \quad j = 1, 2\cdots 5 \tag{45}$$

By the FLS universal approximation capability, the uncertain gain function K_{iu} can be completely expressed by

$$\boldsymbol{K}_{iu} = \boldsymbol{\theta}_{iu}^{*\tau}\boldsymbol{\xi}_{iu}(\boldsymbol{x}) + c_1^* \tag{46}$$

where $\boldsymbol{\theta}_{iu}^*$ is optimal weight parameter, and c_1^* is the ideal approximation error and satisfies $|c_1^*| \leq \overline{c_1}$ with an upper bound $\overline{c_1} > 0$.

C. HEADING CONTROL

Consider the dynamics (2), the heading control τ_{ir} can be chosen as

$$\tau_{ir} = -(\hat{m}_{11} - \hat{m}_{22})\hat{u}_i\hat{v}_i + (\hat{d}_r + \hat{d}_{rr}|\hat{r}_i\|)\hat{r}_i - K_{ir}\,\mathrm{sgn}\,(S_{ir}) - \hat{m}_{33}(\lambda_{i1}\hat{r}_i - \lambda_{i1}\dot{\psi}_{id} - \ddot{\psi}_{id}) \tag{47}$$

where $\lambda_{i1} > 0$; ψ_{id} is the desired heading angle computed by (37), and S_{ir} is the sliding surface governed by

$$S_{ir} = \lambda_{i1}\psi_{ie} + \dot{\psi}_{ie} \tag{48}$$

with $\psi_{ie} = \psi_i - \psi_{id}$. K_{ir} is the uncertain gain function described as

$$\begin{aligned} K_{ir} = &\left((m_{11} - \hat{m}_{11}) + (m_{22} - \hat{m}_{22})\right)\hat{u}_i\hat{v}_i \\ &+ \left(\left(d_r - \hat{d}_r\right) + \left(d_{rr} - \hat{d}_{rr}\right)|\hat{r}_i|\right)\hat{r}_i \\ &+ \left(m_{33} - \hat{m}_{33}\right)\left(\lambda_{i1}\hat{r}_i - \lambda_{i1}\dot{\psi}_{id} - \ddot{\psi}_{id}\right) + \tau_{iwr} \end{aligned} \tag{49}$$

Similarly, a FLS is used to approximate the uncertain dynamics and time-varying disturbances in K_{ir}

$$\hat{K}_{ir} = \hat{\boldsymbol{\theta}}_{ir}^{T}\boldsymbol{\xi}_{ir}(\boldsymbol{x}) \tag{50}$$

where $\hat{\boldsymbol{\theta}}_{ir}$ is adaptive law designed as

$$\dot{\hat{\boldsymbol{\theta}}}_{ir} = \eta_{ir}\,|S_{ir}|\,\boldsymbol{\xi}_{ir}(\boldsymbol{x}) \tag{51}$$

where $\boldsymbol{\eta}_{ir} > 0$; the corresponding membership function is selected as

$$\xi_2^j(\boldsymbol{x}) = \exp\left[-\left(\left(\boldsymbol{x} + \frac{\rho_2}{6} - (j-1)\frac{\rho_2}{12}\right)/\sigma_2\right)^2\right], \quad j = 1, 2\cdots 5 \tag{52}$$

Similar to (46), the unknown K_{ir} can be completely expressed by

$$K_{ir} = \boldsymbol{\theta}_{ir}^{*T}\,\boldsymbol{\xi}_{ir}(\boldsymbol{x}) + c_2^* \tag{53}$$

where $\boldsymbol{\theta}_{ir}^*$ is optimal weight parameter, and c_2^* is the ideal approximation error and satisfies $|c_2^*| \leq \overline{c}_2$ with an upper bound $\overline{c}_2 > 0$.

Theorem 2: Consider the controllers (40) and (47) with FLS (43) and (50), the surge and heading following errors for the *ith* UMV are bounded.

Proof Consider the following FLC as

$$V_{i4} = \frac{1}{2}(m_{33}S_{ir}^2 + m_{11}S_{iu}^2 + \boldsymbol{\eta}_{ir}^{-1}\tilde{\boldsymbol{\theta}}_{ir}^{T}\tilde{\boldsymbol{\theta}}_{ir} + \boldsymbol{\eta}_{iu}^{-1}\tilde{\boldsymbol{\theta}}_{iu}^{T}\tilde{\boldsymbol{\theta}}_{iu}) \tag{54}$$

where $\tilde{\boldsymbol{\theta}}_{ir} = \boldsymbol{\theta}_{ir}^* - \hat{\boldsymbol{\theta}}_{ir}$ and $\tilde{\boldsymbol{\theta}}_{iu} = \boldsymbol{\theta}_{iu}^* - \hat{\boldsymbol{\theta}}_{iu}$ are parameter estimation errors. The time derivate of V_{i4} can be expressed as

$$\begin{aligned} \dot{V}_{i4} &= m_{33}S_{ir}\dot{S}_{ir} + m_{11}S_{iu}\dot{S}_{iu} + \boldsymbol{\eta}_{ir}^{-1}\tilde{\boldsymbol{\theta}}_{ir}^{T}\dot{\tilde{\boldsymbol{\theta}}}_{ir} + \boldsymbol{\eta}_{iu}^{-1}\tilde{\boldsymbol{\theta}}_{iu}^{T}\dot{\tilde{\boldsymbol{\theta}}}_{m} \\ &= S_{ir}(K_{ir} - \hat{K}_{ir}\,\mathrm{sgn}\,(S_{ir})) - \boldsymbol{\eta}_{ir}^{-1}(\boldsymbol{\theta}_{ir}^{*T} - \hat{\boldsymbol{\theta}}_{ir}^{T})\boldsymbol{\eta}_{ir}|S_{ir}|\boldsymbol{\xi}_{ir} \\ &\quad + S_{iu}(K_{iu} - \hat{K}_{iu}\,\mathrm{sgn}\,(S_{iu})) - \boldsymbol{\eta}_{iu}^{-1}(\boldsymbol{\theta}_{iu}^{*T} - \hat{\boldsymbol{\theta}}_{iu}^{T})\boldsymbol{\eta}_{iu}|S_{iu}|\boldsymbol{\xi}_{iu} \\ &\leq S_{ir}K_{ir} - \boldsymbol{\theta}_{ir}^{*T}|S_{ir}|\boldsymbol{\xi}_{ir} + S_{iu}K_{iu} - \boldsymbol{\theta}_{iu}^{*T}|S_{iu}|\boldsymbol{\xi}_{iu} \\ &\leq -\overline{c_1}|S_{ir}| - \overline{c}_2|S_{iu}| \end{aligned} \tag{55}$$

It follows that ψ_{ie} and u_{ie} are bounded as time tends to infinity. This concludes the proof.

VI. STABILITY ANALYSIS

To analyze the underactuated UMV stability in the sway direction, we consider the following FLC as

$$V_v = \frac{1}{2}m_{22}\hat{v}_i^2 \tag{56}$$

From (1) it follows that

$$\dot{V}_v = \hat{v}_i\,(-m_{11}\hat{u}_i\hat{r}_i - d_{22}\hat{v}_i + \tau_{wvi}) \leq -d_{22}\hat{v}_i^2 + \vartheta\,|\hat{v}_i| \tag{57}$$

where $\vartheta = \max(|m_{11}\hat{u}_i\hat{r}_i| + |\tau_{wvi}|)$.

For any $|\hat{v}_i| \geq 2\vartheta/(d_v + d_{vv}|v_i|)$, we have

$$\dot{V}_v \leq -(d_v + d_{vv}|\hat{v}_i|)\hat{v}_i^2/2 \tag{58}$$

Thus, the sway $\hat{v}_i$ is bounded and satisfies

$$|\hat{v}_i(t)| \leq |\hat{v}_i(t_0)|e^{-05d_{33}(t-t_0)} + 2\vartheta/d_{33} \tag{59}$$

Theorem 3: The novel swarm control framework consisting of COS guidance scheme given by (24) (25) (31) together with the control laws (40) (47) renders all signals in the closed-loop swarm system uniformly ultimately bounded.

Proof: Consider the following FLC as

$$V = V_1 + V_3 + \sum\nolimits_{i=1}^{n} V_{i4} \tag{60}$$

Differentiating V along the errors (7) (9) (41) and (48) yields

$$\begin{aligned} &\dot{V} \\ &= \boldsymbol{X}_e^T\boldsymbol{K}_1(\boldsymbol{J}_s(\boldsymbol{\eta})\boldsymbol{V} - \dot{\boldsymbol{X}}_d) + k_3(\partial P/\partial\boldsymbol{\eta})^T\boldsymbol{V} + x_e\dot{x}_e + y_e\dot{y}_e \\ &\quad + \sum_{i=1}^{n}(m_{33}S_{ir}\dot{S}_{ir} + m_{11}S_{iu}\dot{S}_{iu} + \eta_{ir}^{-1}\tilde{\boldsymbol{\theta}}_{ir}^{T}\dot{\tilde{\boldsymbol{\theta}}}_{ir} + \eta_{iu}^{-1}\tilde{\boldsymbol{\theta}}_{iu}^{T}\dot{\tilde{\boldsymbol{\theta}}}_{iu}) \end{aligned}$$

$$
\begin{aligned}
&\leq -(k_3\partial P/\partial \boldsymbol{\eta} + \boldsymbol{J}_S^T\boldsymbol{K}_1\boldsymbol{X}_e)^T(k_3\partial P/\partial \boldsymbol{\eta} + \boldsymbol{J}_s^T\boldsymbol{K}_1\boldsymbol{X}_e) \\
&\quad + \sum_{i=1}^{n}(S_{ir}K_{ir} - \boldsymbol{\theta}_{ir}^{*T}|S_{ir}|\boldsymbol{\xi}_{ir} + S_{iu}K_{iu} - \boldsymbol{\theta}_{iu}^{*T}|S_{iu}|\boldsymbol{\xi}_{iu}) \\
&\quad - \delta x_e^2 - \varepsilon y_e^2 + \Delta \\
&\leq -\boldsymbol{\Gamma}^T\boldsymbol{\Gamma} - \sum_{i=1}^{n}(\overline{c_1}|S_{ir}| + \bar{c}_2|S_{iu}\ \delta x_e^2 - c_l y_e^2 + \Delta \qquad (61)
\end{aligned}
$$

where $\boldsymbol{\Gamma} = k_3\partial P/\partial \boldsymbol{\eta} + \boldsymbol{J}_s^T\boldsymbol{K}_1\boldsymbol{X}_e$ $\Delta = k_3\left|(\partial P/\partial \boldsymbol{\eta})^T\boldsymbol{J}_s^+\dot{\boldsymbol{X}}_d\right|$ and $k_3 > 0$. Thus, it can be concluded that all signals in the closed-loop system are uniformly ultimately bounded. The proof is complete.

VII. SIMULATIONS

Eight UMVs whose dynamics are described by (1) and (2) are used for simulations in MATLAB to demonstrate the effectiveness of the proposed swarm control framework. Each vehicle has the length of 5. 20m, the mass of 1850kg, and the parameters of $m_{11} = 2403$kg, $m_{22} = 3352$kg.$m_{33} = 24896$kg, $d_{11} = 24.5 + 49|u|$kg$/s$, $d_{22} = 584.8 + 453.8|v|kg/s$, $d_{33} = 1827.8 + 1800|r|kg/s$.

The time-varying disturbances are assumed as follows:

$$
\tau_{wui} = [m_{11}\vartheta_1, m_{22}\vartheta_2, m_{33}\vartheta_3]^T \qquad (62)
$$

where ϑ_1, ϑ_2 and ϑ_3 are zero-mean Gaussian white noise processes.

The initial dynamics of each UMV is defined as $v_i = [0, 0, 0]^T$ and kinematics is as follows:

$$
\begin{cases}
\boldsymbol{\eta}_1 = [-80, 50, 0.25\pi]^T, & \boldsymbol{\eta}_2 = [80, 40, 0.25\pi]^T \\
\boldsymbol{\eta}_3 = [-40, -20, 0.5\pi]^T, & \boldsymbol{\eta}_4 = [-80, 100, 0]^T \\
\boldsymbol{\eta}_5 = [20, -20, 0]^T, & \boldsymbol{\eta}_6 = [0, 20, 0.5\pi]^T \\
\boldsymbol{\eta}_7 = [200, -100, 0.65\pi]^T, & \boldsymbol{\eta}_8 = [150, -60, 0.5\pi]^T
\end{cases} \qquad (63)
$$

The desired velocity is $10kn$ and the desired standard deviation σ_d is $50m$. Moreover, the desired path is parameterized by

$$
\begin{cases}
x_d(\theta) = \theta \\
y_d(\theta) = 200^* \sin(\pi\theta/400)
\end{cases} \qquad (64)
$$

where θ is managed by

$$
\dot{\theta} = \frac{u_p}{\sqrt{\dot{x}_d^2(\theta) + \dot{y}_d^2(\theta)}} \qquad (65)
$$

and u_p is defined by (14).

For obstacle avoidance, the distances are designed as $d_0 = 30$, $D_0 = 90$, $D_1 = 60$. The COS guidance is designed as

$$
\begin{cases}
\boldsymbol{V}_d = -(k_3\partial P/\partial \boldsymbol{\eta} + \boldsymbol{J}_s^T\boldsymbol{K}_1\boldsymbol{X}_e) + \boldsymbol{J}_s^+\dot{\boldsymbol{X}}_d \\
P = k_1\sum_{i=1}^{m} P_{aoi} + k_2\sum_{i=1}^{n} P_{ari}
\end{cases} \qquad (66)
$$

with parameters $k_1 = 20$, $k_2 = 15$, and $k_3 = 2$.

The distributed and self-organized swarm control framework is shown in Fig. 3.

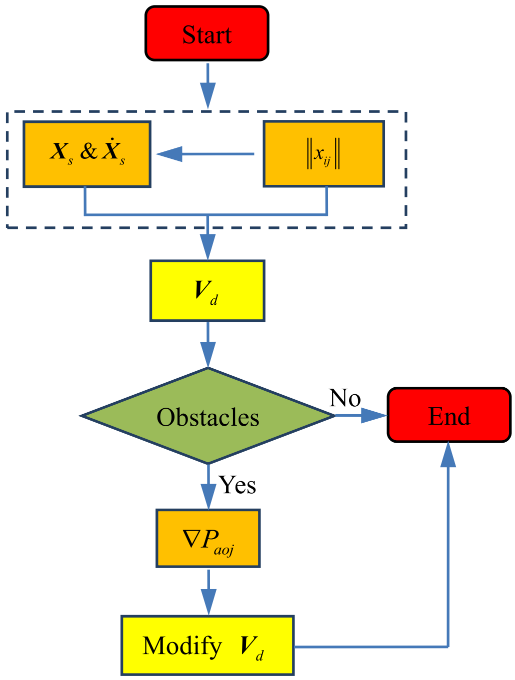

FIGURE 3. Swarm control framework.

The gains in the controllers and the guidance scheme are chosen as follows: $\boldsymbol{K}_1 = diag(0.1, 0.1, 0.1)$, $\delta = 0.2$, $l_0 = 20$, $\lambda_{i1} = 0.4$, $\lambda_{i2} = 5$, $\eta_{iu} = \eta_{ir} = 500$, $\alpha = 2.5$, $\beta = 4$. Considering controller hysteresis and turning radius constraint, swarm errors satisfy that $\varepsilon_{i=1,2,3} = 5.2m$ (the length of vehicle).

There are three challenges in the swarm path following: (1) the large number vehicles; (2) the large initial errors; and (3) the fast response to the obstacles. However, these challenges are addressed reasonably and effectively using the proposed swarm control framework. The swarm following performance of multiple UMVs is shown in Fig. 4 $(a) - (e)$, from which we can see that each vehicle can follow the desired path. Moreover, collision avoidance and obstacle avoidance for multiple UMVs in the presence of uncertain dynamics and unmeasured velocities are addressed. In particular, Fig. 4 (c) and Fig. 4 (d) show that each UMV can bypass obstacles in black color smoothly with safe distance. From Fig. 5, it is apparent that the following errors x_e, y_e and $\sigma - \sigma_d$ with COS guidance scheme can converge smoothly to zero. However, UMVs must take measures to keep away from obstacles at time 150s to 200s, and the following errors cannot converge to zero, which are reasonable. Fig.6 shows the 6th UMV surge velocity u_6 and yaw angle ψ_6 by proposed scheme, and it also demonstrates that each UMV can make good progress with 10kn towards the desired path. Fig. 7 shows the control signals of the 6th UMV. Fig. 8 shows that unknown velocity information can be accurately estimated by the proposed observer.

In summary, the swarm control framework with COS guidance and fuzzy sliding mode can achieve cooperative path following in the presence of uncertain dynamics and time-varying disturbances.

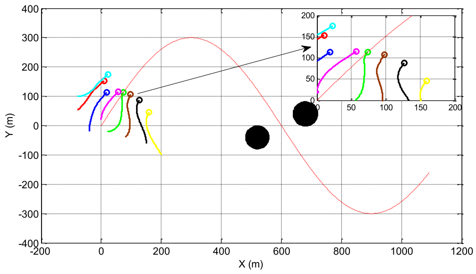

a. At time t=25 sec

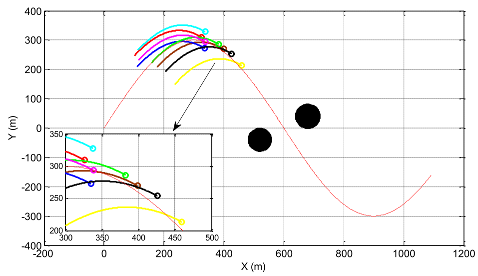

b. At time t=100 sec

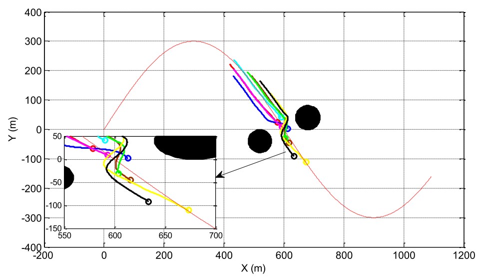

c. At time t=175 sec

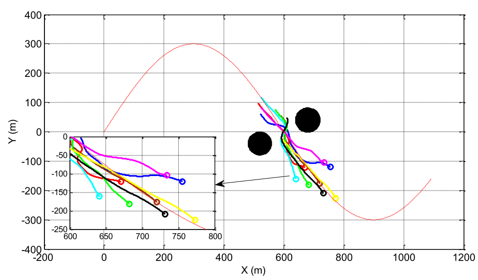

d. At time t=200 sec

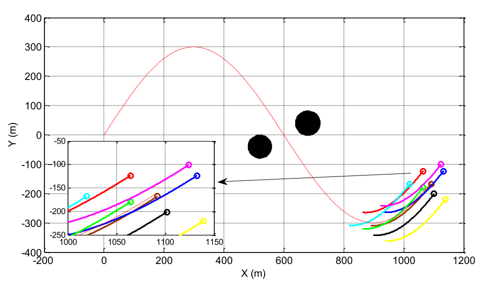

e At time t=300 sec

FIGURE 4. Swarm following performance for eight UMVs.

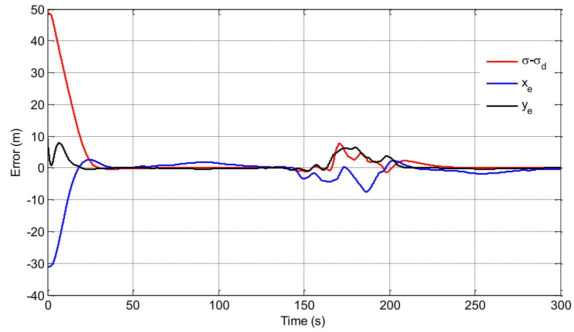

FIGURE 5. Swarm following errors.

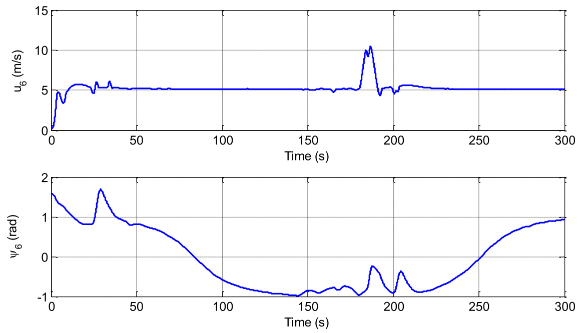

FIGURE 6. Surge speed and heading angle for the 6th UMV.

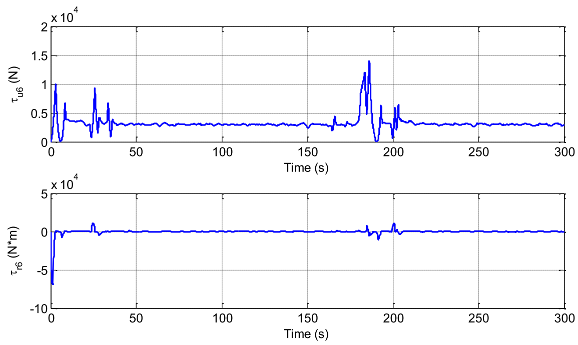

FIGURE 7. Control inputs for the 6th UMV.

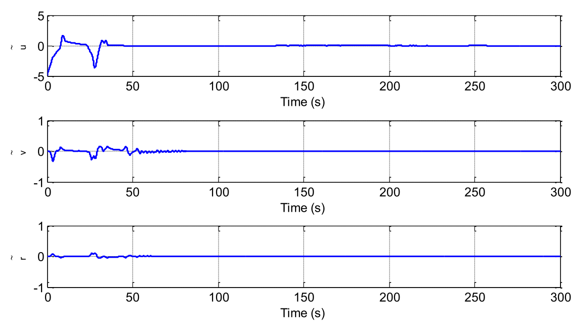

FIGURE 8. Velocity observation errors for the 6th UMV.

VIII. CONCLUSION

In this paper, the problem of swarm-based path following for multiple UMVs has been addressed. By virtue of the SOC guidance and the improved APF, a distributed and self-organized swarm control framework is employed. The unmeasured velocities and time-varying disturbances have been proposed by velocity observer and fuzzy sliding mode control, respectively, which can ensure all signals in the closed-loop system are bounded. Moreover, swarm path following performance is proven by simulations. The obstacles considered in this paper are static, and hence, future researches focus on the dynamic cases.

REFERENCES

[1] Y. Lu, G. Q. Zhang, Z. Sun, and W. D. Zhang, "Adaptive cooperative formation control of autonomous surface vessels with uncertain dynamics and external disturbances," *Ocean Eng.*, vol. 167, pp. 36–44, Nov. 2018.

[2] N. Wang, Z. Sun, Z. Zheng, and H. Zhao, "Finite-time sideslip observer-based adaptive fuzzy path-following control of underactuated marine vehicles with time-varying large sideslip," *Int. J. Fuzzy Syst.*, vol. 20, no. 6, pp. 1767–1778, Aug. 2018.

[3] R. B. Wynn, V. A. I. Huvenne, T. P. L. Bas, B. J. Murton, D. P. Connelly, B. J. Bett, H. A. Ruhl, K. J. Morris, J. Peakall, D. R. Parsons, E. J. Sumner, S. E. Darby, and J. E. Hunt, R. M. Dorrell, "Autonomous underwater vehicles (AUVs): Their past, present and future contributions to the advancement of marine geoscience," *Mar. Geol.*, vol. 352, pp. 451–468, Jun. 2014.

[4] X. Liang, Y. Li, Z. Peng, and J. Zhang, "Nonlinear dynamics modeling and performance prediction for underactuated AUV with fins," *Nonlinear Dyn.*, vol. 84, no. 1, pp. 237–247, Apr. 2016.

[5] J. Wang, J.-Y. Liu, and H. Yi, "Formation control of unmanned surface vehicles with sensing constraints using exponential remapping method," *Math. Problem Eng.*, vol. 2017, Aug. 2017, Art. no. 7619086.

[6] H. Mehrjerdi, J. Ghomman, and M. Saan, "Nonlinear coordination control for a group of mobile robots using a virtual structure," *Mechatronics*, vol. 21, no. 7, pp. 1147–1155, Oct. 2011.

[7] K. Kanjanawanishkul, "Coordinated path following for mobile robots using a virtual structure strategy with model predictive control," *Automatika*, vol. 55, no. 3, pp. 287–298, Sep. 2015.

[8] J. Chen, M. Gan, J. Huang, L. Dou, and H. Fang, "Formation control of multiple Euler-Lagrange systems via null-space-based behavioral control," *Sci. China Inf. Sci.*, vol. 59, no. 1, pp. 1–11, 2016.

[9] G. Lee and D. Chwa, "Decentralized behavior-based formation control of multiple robots considering obstacle avoidance," *Intell. Service Robot.*, vol. 11, no. 1, pp. 127–138, 2018.

[10] R. Cui, S. S. Ge, B. V. E. How, and Y. S. Choo, "Leader–follower formation control of underactuated autonomous underwater vehicles," *Ocean Eng.*, vol. 37, nos. 17–18, pp. 1491–1502, Dec. 2010.

[11] D. J. W. Belleter and K. Y. Pettersen, "Underactuated leader-follower synchronisation for multi-agent systems with rejection of unknown disturbances," in *Proc. IEEE Conf. Amer. Control*, Chicago, IL, USA, Jul. 2015, pp. 3094–3100.

[12] A. Loria, J. Dasdemir, and N. A. Jarquin, "Leader-Follower formation and tracking control of mobile robots along straight paths," *IEEE Trans. Control Syst. Technol.*, vol. 24, no. 2, pp. 727–732, Mar. 2016.

[13] H. Wang, D. Guo, X. Liang, W. Chen, G. Hu, and K. K. Leang, "Adaptive vision-based leader–follower formation control of mobile robots," *IEEE Trans. Ind. Electron.*, vol. 64, no. 4, pp. 2893–2902, Apr. 2017.

[14] H. Mehrjerdi, M. Saad, M, J. Ghommam, and A. Zerigui, "Formation and path following for multiple mobile robots," in *Proc. IEEE Int. Symp. Ind. Electron.*, Bari, Italy, Jul. 2010, pp. 1864–1868.

[15] F. Valenciaga, "A second order sliding mode path following control for autonomous surface vessels," *Asian J. Control*, vol. 16, no. 5, pp. 1515–1521, Sep. 2014.

[16] T. Elmokadem, M. Zribi, and K. Youcef-Toumi, "Trajectory tracking sliding mode control of underactuated AUVs," *Nonlinear Dyn.*, vol. 84, no. 2, pp. 1079–1091, Apr. 2016.

[17] Z. Sun, G. Zhang, Y. Lu, and W. Zhang, "Leader-follower formation control of underactuated surface vehicles based on sliding mode control and parameter estimation," *ISA Trans.*, vol. 72, pp. 15–24, Jan. 2018.

[18] R. Rout and B. Subudhi, "A backstepping approach for the formation control of multiple autonomous underwater vehicles using a leader–follower strategy," *J. Marine Eng. Technol.*, vol. 15, no. 1, pp. 38–46, 2016.

[19] S. Emrani, A. Dirafzoon, and H. A. Talebi, "Leader-follower formation control of autonomous underwater vehicles with limited communications," in *Proc. IEEE Conf. CCA*, Denver, CO, USA, Sep. 2011, pp. 921–926.

[20] Z. Peng, D. Wang, Z. Chen, X. Hu, and W. Lan, "Adaptive dynamic surface control for formations of autonomous surface vehicles with uncertain dynamics," *IEEE Trans. Control Syst. Technol.*, vol. 21, no. 2, pp. 513–520, Mar. 2013.

[21] L. Eski and S. Yildirim, "Design of neural network control system for controlling trajectory of autonomous underwater vehicles," *Int. J. Adv. Robotic Syst.*, vol. 11, no. 7, p. 17, Jan. 2014.

[22] G. Ding, D. Zhu, and B. Sun, "Formation control and obstacle avoidance of multi-AUV for 3-D underwater environment," in *Proc. Chin. Control Conf.*, Nanjing, China, Jul. 2014, pp. 8347–8352.

[23] J. Ji, A. Khajepour, W. W. Melek, and Y. Huang, "Path planning and tracking for vehicle collision avoidance based on model predictive control with multiconstraints," *IEEE Trans. Ultrason. Eng.*, vol. 66, no. 2, pp. 952–964, Feb. 2017.

[24] L. Palacios, M. Ceriotti, and G. Radice, "Close proximity formation flying via linear quadratic tracking controller and artificial potential function," *Adv. Space Res.*, vol. 56, no. 10, pp. 2167–2176, Nov. 2015.

[25] Y.-C. Liu and N. Chopra, "Control of semi-autonomous teleoperation system with time delays," *Automatica*, vol. 49, no. 6, pp. 1553–1565, 2013.

[26] E. Oland and R. Kristiansen, "Collision and terrain avoidance for UAVs using the potential field method," in *Proc. IEEE Aerosp. Conf.*, Big Sky, MT, USA, Mar. 2013, pp. 1–7.

[27] J. Sun, J. Tang, and S. Lao, "Collision avoidance for cooperative UAVs with optimized artificial potential field algorithm," *IEEE Access*, vol. 5, pp. 18382–18390, 2017.

[28] G. V. Lakhekar and L. M. Waghmare, "Adaptive fuzzy exponential terminal sliding mode controller design for nonlinear trajectory tracking control of autonomous underwater vehicle," *Int. J. Dyn. Control*, vol. 6, no. 4, pp. 1690–1705, Dec. 2018.

[29] P. S. Londhe and B. M. Patre, "Adaptive fuzzy sliding mode control for robust trajectory tracking control of an autonomous underwater vehicle," *Intell. Service Robot.*, vol. 12, no. 1, pp. 87–102, Jan. 2019.

[30] B. K. Sahu and B. Subudhi, "Flocking control of multiple AUVs based on fuzzy potential functions," *IEEE Trans. Fuzzy Syst.*, vol. 26, no. 5, pp. 2539–2551, Oct. 2018.

[31] Z. Qin, Z. Lin, D. M. Yang, and P. Li, "A task-based hierarchical control strategy for autonomous motion of an unmanned surface vehicle swarm," *Appl. Ocean Res.*, vol. 65, pp. 251–261, Apr. 2017.

[32] N. Wang, Z. Sun, J. Yin, S.-F. Su, and S. Sharma, "Finite-time observer based guidance and control of underactuated surface vehicles with unknown sideslip angles and disturbances," *IEEE Access*, vol. 6, pp. 14059–14070, 2018.

[33] W. Kowalczyk, M. Michalek, and K. Kozłowski, "Trajectory tracking control and obstacle avoidance for a differentially driven mobile robot," in *Proc. 18th World Congr. Autom. Control*, Milano, Italy, Aug. 2011, pp. 1058–1063.

[34] Z. H. Peng, D. Wang, W. Lan, G. Sun, and L. Yan, "Neural adaptive flocking control of networked underactuated autonomous surface vehicles in the presence of uncertain dynamics," in *Proc. 31st Chin. Control Conf.*, Hefei, China, Jul. 2012, pp. 2865–2870.

[35] X. Liang, X. Qu, L. Wan, and Q. Ma, "Three-dimensional path following of an underactuated AUV based on fuzzy backstepping sliding mode control," *Int. J. Fuzzy Syst.*, vol. 20, no. 2, pp. 640–649, 2018.

[36] N. Wang, Z. Sun, J. Yin, Z. Zou, and S.-F. Su, "Fuzzy unknown observer-based robust adaptive path following control of underactuated surface vehicles subject to multiple unknowns," *Ocean Eng.*, vol. 176, pp. 57–64, Mar. 2019.

XIAO LIANG received the degree in naval architecture and ocean engineering from Harbin Engineering University, China, in 2003, the M.S. degree in fluid mechanics from Harbin Engineering University, in 2006, and the Ph.D. degree in design and construction of naval architecture and ocean structure, in 2009. He is currently a Professor with the School of Naval Architecture and Ocean Engineering, Dalian Maritime University, China. He has authored and co-authored more than 60 papers in scientific journals. His current research interests include intelligent control and simulation of unmanned marine vehicles.

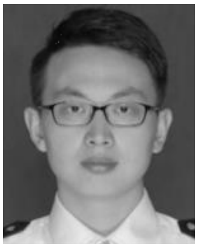

XINGRU QU received the B.E. and M.E. degrees in naval architecture and ocean engineering from Shandong Jiaotong University, Jinan, China, in 2015, and Dalian Maritime University, Dalian, China, in 2018, respectively, where he is currently pursuing the Ph.D. degree in naval architecture and ocean engineering. His current research activities are focused on intelligent control and simulation for unmanned marine vehicles.

NING WANG (S'08–M'12–SM'15) received the B.Eng. degree in marine engineering and the Ph.D. degree in control theory and engineering from Dalian Maritime University (DMU), Dalian, China, in 2004 and 2009, respectively. From 2008 to 2009, he was a joint-training Ph.D. student with Nanyang Technological University, Singapore, where he was financially supported by the China Scholarship Council. He is currently an Associate Professor with the Marine Engineering College, DMU. His current research interests include fuzzy logic systems, artificial neural networks, machine learning, self-organizing fuzzy neural modeling and control ship intelligent control, and dynamic ship navigational safety assessment. He was a recipient of the Nomination Award of Liaoning Province Excellent Doctoral Dissertation, the DMU Excellent Doctoral Dissertation Award and the DMU Outstanding Ph.D. Student Award in 2010, the Excellent Government-Funded Scholars and the Students Award in 2009, the Liaoning Province Award for Technological Invention, the Honour of Liaoning BaiQianWan Talents, the Liaoning Excellent Talents, Science and Technology Talents the Ministry of Transport of the PRC, Youth Science and Technology Award of China Institute of Navigation, and the Dalian Leading Talents. He currently serves as an Associate Editor for the *Neurocomputing*.

YE LI received the degree in naval architecture and ocean engineering from Harbin Engineering University, China, in 2001, and the M.S. and Ph.D. degrees in design and construction of naval architecture and ocean structure from Harbin Engineering University, in 2004 and 2007, respectively. He is currently a Professor with the Science and Technology on Underwater Vehicle Technology, China. He has authored and co-authored more than 140 papers in scientific journals. His current research interests include navigation technology and intelligent control for autonomous underwater vehicles.

RUBO ZHANG is currently a Professor and the Ph.D. supervisor with Dalian Minzu University. His research interests include intelligent robot, computing intelligence, machine learning, and machine perception.